Evaluating platelet aggregation dynamics from laser speckle fluctuations

ZEINAB HAJJARIAN, DIANE M. TSHIKUDI, AND SEEMANTINI K. NADKARNI[*]

Wellman Center for Photomedicine, Massachusetts General Hospital and Harvard Medical School, 40 Blossom Street, Boston, MA 02114, USA
[*]*snadkarni@mgh.harvard.edu*

Abstract: Platelets are key to maintaining hemostasis and impaired platelet aggregation could lead to hemorrhage or thrombosis. We report a new approach that exploits laser speckle intensity fluctuations, emanated from a drop of platelet-rich-plasma (PRP), to profile aggregation. Speckle fluctuation rate is quantified by the speckle intensity autocorrelation, $g_2(t)$, from which the aggregate size is deduced. We first apply this approach to evaluate polystyrene bead aggregation, triggered by salt. Next, we assess dose-dependent platelet aggregation and inhibition in human PRP spiked with adenosine diphosphate and clopidogrel. Additional spatio-temporal speckle analyses yield 2-dimensional maps of particle displacements to visualize platelet aggregate foci within minutes and quantify aggregation dynamics. These findings demonstrate the unique opportunity for assessing platelet health within minutes for diagnosing bleeding disorders and monitoring anti-platelet therapies.

References and links

1. D. J. Angiolillo, M. Ueno, and S. Goto, "Basic principles of platelet biology and clinical implications," Circ. J. **74**(4), 597–607 (2010).
2. L. Brass, "Understanding and Evaluating Platelet Function," Hematology (Am Soc Hematol Educ Program) **2010**(1), 387–396 (2010).
3. A. D. Michelson, "Methods for the measurement of platelet function," Am. J. Cardiol. **103**(3 Suppl), 20A–26A (2009).
4. S. M. Picker, "In-vitro assessment of platelet function," Transfus. Apheresis Sci. **44**(3), 305–319 (2011).
5. G. V. R. Born, "Aggregation of Blood Platelets by Adenosine Diphosphate and Its Reversal," Nature **194**(4832), 927–929 (1962).
6. J. R. O'Brien, "The adhesiveness of native platelets and its prevention," J. Clin. Pathol. **14**(2), 140–149 (1961).
7. M. Cattaneo, C. Cerletti, P. Harrison, C. P. Hayward, D. Kenny, D. Nugent, P. Nurden, A. K. Rao, A. H. Schmaier, S. P. Watson, F. Lussana, M. T. Pugliano, and A. D. Michelson, "Recommendations for the Standardization of Light Transmission Aggregometry: A Consensus of the Working Party from the Platelet Physiology Subcommittee of SSC/ISTH," J. Thromb. Haemost. **11**(6), 1183–1189 (2013).
8. M. Cattaneo, C. P. Hayward, K. A. Moffat, M. T. Pugliano, Y. Liu, and A. D. Michelson, "Results of a World-wide Survey on the Assessment of Platelet Function by Light Transmission Aggregometry: a Report from the Platelet Physiology Subcommittee of the Scientific and Standardization Committee of the International Society on Thrombosis and Haemostasis," J. Thromb. Haemost. **7**, 1029 (2009).
9. C. Corredor, M. Wasowicz, K. Karkouti, and V. Sharma, "The role of point-of-care platelet function testing in predicting postoperative bleeding following cardiac surgery: a systematic review and meta-analysis," Anaesthesia **70**(6), 715–731 (2015).
10. L. Zhou and A. H. Schmaier, "Platelet Aggregation Testing in Platelet-Rich Plasma: description of procedures with the aim to develop standards in the field," Am. J. Clin. Pathol. **123**(2), 172–183 (2005).
11. Z. Hajjarian, M. M. Tripathi, and S. K. Nadkarni, "Optical Thromboelastography to evaluate whole blood coagulation," J. Biophotonics **8**(5), 372–381 (2015).
12. M. M. Tripathi, Z. Hajjarian, E. M. Van Cott, and S. K. Nadkarni, "Assessing blood coagulation status with laser speckle rheology," Biomed. Opt. Express **5**(3), 817–831 (2014).
13. N. G. Sultanova, S. N. Kasarova, and I. D. Nikolov, "Characterization of optical properties of optical polymers," Opt. Quantum Electron. **45**(3), 221–232 (2013).
14. M. Meinke, G. Müller, J. Helfmann, and M. Friebel, "Optical properties of platelets and blood plasma and their influence on the optical behavior of whole blood in the visible to near infrared wavelength range," J. Biomed. Opt. **12**, 014024 (2007).

15. Z. Hajjarian and S. K. Nadkarni, "Evaluating the viscoelastic properties of tissue from laser speckle fluctuations," Sci. Rep. **2**, 316 (2012).
16. Z. Hajjarian and S. K. Nadkarni, "Evaluation and correction for optical scattering variations in laser speckle rheology of biological fluids," PLoS One **8**(5), e65014 (2013).
17. Z. Hajjarian and S. K. Nadkarni, "Correction of optical absorption and scattering variations in laser speckle rheology measurements," Opt. Express **22**(6), 6349–6361 (2014).
18. T. J. Farrell, M. S. Patterson, and B. Wilson, "A diffusion theory model of spatially resolved, steady-state diffuse reflectance for the noninvasive determination of tissue optical properties in vivo," Med. Phys. **19**(4), 879–888 (1992).
19. T. G. Mason, H. Gang, and D. A. Weitz, "Diffusing-wave-spectroscopy measurements of viscoelasticity of complex fluids," J. Opt. Soc. Am. A **14**(1), 139–149 (1997).
20. G. Késmárky, P. Kenyeres, M. Rábai, and K. Tóth, "Plasma viscosity: a forgotten variable," Clin. Hemorheol. Microcirc. **39**(1-4), 243–246 (2008).
21. A. A. Weber, S. Reimann, and K. Schrör, "Specific inhibition of ADP-induced platelet aggregation by clopidogrel in vitro," Br. J. Pharmacol. **126**(2), 415–420 (1999).
22. R. Shaw, "Dynamic Light Scattering Training," (Malvern Instruments Ltd, 2014).
23. M. A. Dobrovolskaia, A. K. Patri, J. Simak, J. B. Hall, J. Semberova, S. H. De Paoli Lacerda, and S. E. McNeil, "Nanoparticle size and surface charge determine effects of PAMAM dendrimers on human platelets in vitro," Mol. Pharm. **9**(3), 382–393 (2012).
24. D. Özsavcı, A. Şener, R. Oba, G. Yanıkkaya Demirel, F. Uras, and T. K. Yardımcı, "New in vitro effects of clopidogrel on platelets in hyperlipidemic and healthy subjects," Turk. J. Haematol. **27**(2), 99–108 (2010).
25. V. L. Serebruany, S. R. Steinhubl, P. B. Berger, A. I. Malinin, J. S. Baggish, D. L. Bhatt, and E. J. Topol, "Analysis of risk of bleeding complications after different doses of aspirin in 192,036 patients enrolled in 31 randomized controlled trials," Am. J. Cardiol. **95**(10), 1218–1222 (2005).
26. C. H. Kicken, M. Roest, Y. M. Henskens, B. de Laat, and D. Huskens, "Application of an optimized flow cytometry-based quantification of Platelet Activation (PACT): Monitoring platelet activation in platelet concentrates," PLoS One **12**(2), e0172265 (2017).
27. D. Aradi, A. Tornyos, T. Pintér, A. Vorobcsuk, A. Kónyi, J. Falukozy, G. Veress, B. Magyari, I. G. Horváth, and A. Komócsi, "Optimizing P2Y12 receptor inhibition in patients with acute coronary syndrome on the basis of platelet function testing: impact of prasugrel and high-dose clopidogrel," J. Am. Coll. Cardiol. **63**(11), 1061–1070 (2014).
28. J. A. Jakubowski, Y. G. Li, D. S. Small, C. D. Payne, M. E. Tomlin, J. Luo, and K. J. Winters, "A comparison of the VerifyNow P2Y12 point-of-care device and light transmission aggregometry to monitor platelet function with prasugrel and clopidogrel: an integrated analysis," J. Cardiovasc. Pharmacol. **56**(1), 29–37 (2010).
29. H. L. Nielsen, S. D. Kristensen, S. S. Thygesen, J. Mortensen, S. B. Pedersen, E. L. Grove, and A. M. Hvas, "Aspirin response evaluated by the VerifyNow Aspirin System and light transmission aggregometry," Thromb. Res. **123**(2), 267–273 (2008).
30. A. J. Wikkelsoe, A. Afshari, J. Wetterslev, J. Brok, and A. M. Moeller, "Monitoring patients at risk of massive transfusion with Thrombelastography or Thromboelastometry: a systematic review," Acta Anaesthesiol. Scand. **55**(10), 1174–1189 (2011).

1. Introduction

Platelets play key roles in hemostasis and in maintaining the balance between bleeding and coagulation [1]. Upon vascular injury, and during the initial phase of coagulation, multiple surface receptors mediate the adhesion of platelets to exposed collagen on the injured endothelium [1]. The subsequent arrest and activation of platelets prompt conformational changes and expression of pro-coagulant factors [2]. The activated platelets then aggregate to form a stable hemostatic plug, which is later superimposed, and stabilized by the fibrin mesh, entrapping circulating red blood cells, to restrict bleeding [1]. Platelet dysfunctions are often associated with hereditary and acquired bleeding disorders and are the underlying cause of life-threatening bleeding or thromboembolic conditions. As such, evaluating different aspects of platelet function during coagulation is critical for diagnosing coagulopathies, monitoring antiplatelet therapies, determining the thrombosis susceptibility in patients with coronary and peripheral artery diseases, and for monitoring the health of stored platelets [3].

Automated and standardized lab tests to measure prothrombin time (PT), activated partial thromboplastin time (aPTT), or coagulation factor levels enable for screening common coagulation defects of the secondary hemostasis pathways. However, platelet function deficiencies, related to primary hemostasis, remain difficult to diagnose even within the lab setting given the high cost and time considerations, requirements for large sample volumes and specialized equipment, as well as trained personnel [2–4]. Traditionally, the diagnosis of platelet-related

coagulation defects has been limited to platelet count and morphological analysis, which lack the sensitivity and specificity to detect platelet dysfunction [4]. The only widely adopted lab test for functional platelet assessment, light transmission aggregometry (LTA), was developed over 50 years ago [5, 6]. In LTA, light transmitted through a platelet-rich plasma (PRP) specimen is measured to assess the relative plasma "turbidity" as an indirect indicator of platelet aggregation, upon spiking with varying doses of agonists, such as Adenosine 5′-diphosphate (ADP), collagen, epinephrine, ristocetin, serotonin, thromboxane A2 (TxA2), and thrombin. Nevertheless, LTA is a labor and time-intensive approach, requiring large volumes of blood (~8mL) and PRP, has low sensitivity in measuring small platelet aggregation changes, and therefore often lacks the sensitivity and specificity required for early diagnosis of platelet dysfunction in patients [7, 8].

In recent years, several new techniques have been developed for testing platelet function. Yet, most of the proposed instruments are bulky, require specialized operators and have a high cost of instrumentation and disposables, and as a result have low clinical adoption rates, as discussed later [2, 3, 9]. Therefore, there is clearly a demand for novel and inexpensive functional tests that can be conveniently adopted in the clinical setting for detecting platelet deficiencies and evaluating the response to anti-platelet agents at the patient's bedside. In this paper, we exploit a laser speckle approach for evaluating platelet function related to primary hemostasis using a small volume of PRP. In this approach, a PRP specimen (~120µl) is illuminated by a laser source and temporally fluctuating speckle patterns are captured by a high-speed CMOS sensor. Due to its capacity for assessing platelet function in a small sample volume of only 120 µl, the laser speckle approach is at major advantage for translation to point of care. Since the plasma specimen is anti-coagulated, fibrin generation is inhibited. As such, the unrestricted Brownian excursions of platelets throughout the primarily viscous homogeneous plasma induce evenly paced, nearly ergodic, temporal speckle intensity fluctuations. Prior to activation via a platelet agonist, agile movements of individual platelets prompt rapid speckle modulations. Soon after spiking with agonists, Brownian dynamics are altered according to key aspects of platelets function particularly due to platelet aggregation, which ultimately culminate in platelet plug formation. The aggregate growth slows down the Brownian displacements and decelerates speckle fluctuations.

Here, we exploit the high sensitivity of laser speckle intensity fluctuations to the kinetics of scattering particles to closely track the phases of platelet aggregation during primary hemostasis and demonstrate the potential of this approach for functional platelet testing. To this end, we detail methods for measuring the platelet kinetics and discuss results obtained using phantoms composed of polystyrene bead suspensions and human PRP specimens, spiked with varying doses of a platelet agonist and an anti-platelet agent.

2. Materials and methods

2.1 Polystyrene bead suspensions

We first demonstrated the utility of laser speckle fluctuations for evaluating the aggregation dynamics in polystyrene microsphere suspensions. Inorganic salts were used to trigger the aggregation and clumping of polystyrene bead by changing their surface chemistry. More specifically, the surfaces of polystyrene beads in suspensions are negatively charged to prevent agglutination and aggregation. In the presence of a salt buffer, the individual salt ions bind to and neutralize the anionic charges on the bead surface, eliminating electrostatic barriers and prompting particle aggregation to various extents depending on the salt concentration. In the current study, 50 µl of polystyrene microsphere suspensions (1.5µm dia., 2.5% solid volume concentration, Polysciences, Inc.) were mixed with 150 µl of $MgCl_2$ solutions of 0, 5, 45, and 300 µM molar concentrations to initiate particle clumping at different aggregation rates. Based on the initial size and concentration of poly beads, Mie theory calculations returned the reduced scattering coefficient, μ_s', of 1.6 mm^{-1} and an absorption coefficient of $\mu_a = 0$ mm^{-1},

for all specimens. Nevertheless, as expected, the samples became increasingly less turbid, once the aggregation process started. The poly-bead plus salt solutions were loaded in imaging chambers (Grace Bio-Labs Inc., USA), which consisted of a cylindrical enclosure to house the specimen (9 mm Dia., 2 mm thickness) and a clear poly-carbonate window, and speckle acquisition started immediately as described below.

2.2 Human PRP specimens

Next, we tested and verified the potential of exploiting laser speckle intensity fluctuations for the accurate and sensitive detection of platelet activation, aggregation, inhibition, and monitoring the change of effective aggregate size in PRP specimens obtained from patients, and spiked with combinations of platelet agonist ADP, and the anti-platelet agent clopidogrel bisulphate (Plavix®). ADP is a mild agonist that targets the $P2Y_1$ and $P2Y_{12}$ platelet receptors. The $P2Y_1$ receptor is responsible for platelet shape changes and the primary wave of aggregation. The $P2Y_{12}$ receptor, on the other hand, mediates the secondary phase of aggregation and is the major target of the anti-platelet drug, clopidogrel [10].

To prepare the 4660 µM clopidogrel stock solution, a Plavix® tablet (75 mg, Bristol-Meyer Squibb) was crushed to powder, mixed with 50 ml of deionized water, sonicated for 10 minutes, and incubated at 50° C in a water bath for 3 minutes. Following institutional review board (IRB) approval, de-identified blood specimens from two patients undergoing routine coagulation testing were collected in 0.105 M sodium citrate vacutainer system (Becton & Dickinson, Co., Franklin Lakes, NJ, USA) from the MGH special coagulation laboratory. The specimens were centrifuged at 1000 rpm to obtain the PRP. One PRP specimen was divided into four samples of 250 µl. The first sample (control) was mixed with 7.86 µl of saline. The second sample was mixed 1.61 µl of saline and 6.25 µl of ADP stock solution (200 µM, Helena Laboratories, Beaumont, TX, USA) to attain a 5µM ADP concentration. In the third sample, 6.25 µl of ADP and 1.61 µl of diluted clopidogrel (10 × dilution, 466 µM) were mixed in, leading to 5 and 3 µM concentrations of ADP and clopidogrel, respectively. Finally, 6.25 µl of ADP and 1.61 µl of clopidogrel (un-diluted, 4660 µM) were mixed with the fourth 250 µl plasma specimen leading to 5 and 30 µM concentrations of ADP and clopidogrel, respectively. The PRP specimen from the second patient was split into two 250 µl samples. The control sample was mixed with 12.5 µl of saline, whereas the test sample was spiked with 12.5 µl of ADP, i.e. 10 µM concentration. To measure platelet aggregation, 120 µl of the samples were loaded in imaging chambers and speckle image acquisition started promptly.

2.3 Laser speckle acquisition

The optical setup, used to acquire speckle intensity fluctuations, is presented in Fig. 1(a) [11, 12]. In short, light from a He-Ne laser source (9 mW output power, 632nm wavelength) was linearly polarized and brought to focus by a beam splitter and a lens to a 50 µm spot on the samples, delivering a total power of 2 mW, corresponding to an irradiance of 1000 mW/mm2. Due to the negligible absorption coefficient of the test specimens, (i.e. $\mu_a \sim 0$ for polystyrene bead suspensions and 0.00165 mm^{-1} for platelet rich plasma at 632 nm), any temperature rise during imaging within the samples was insignificant [13, 14]. We further tested the temperature stability of the specimens during imaging and confirmed that the temperature difference between the illuminated (test) and non-illuminated (control) specimens was negligible (discussed below). A high-speed camera (Basler, Ace 2000-340 km), equipped with a Macro-lens (Computar, MLH-10 ×) and configured in 180° back-scattering geometry acquired the cross-polarized speckle patterns. This collection geometry eliminated majority of the static speckle, induced by specular reflection from the imaging chamber and significantly simplified the interpretation of speckle intensity fluctuations. Any residual non-fluctuating background component was further eliminated from the speckle time series as discussed later. The iris opening of the Macro-lens was adjusted to map a single speckle spot to 5 × 5 pixels. The pixel to

speckle ratio was verified by evaluating the spatial autocorrelation function of speckle images and calculating the spatial correlation distance, which was about 5 pixels.
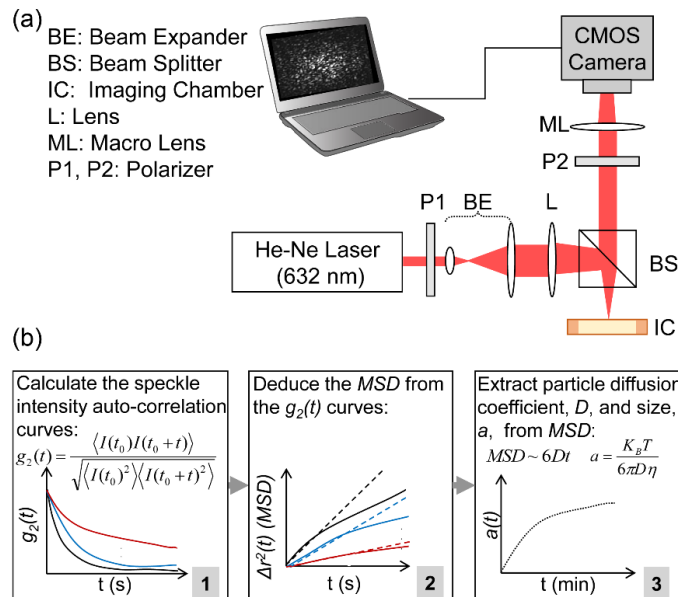

Fig. 1. (a) Schematic diagram of the optical setup. Laser beam is linearly polarized and focused at the sample site. The backscattered rays are collected through a second polarizer and imaged at the CMOS camera sensor. (b) Block diagram of the speckle dynamic processing algorithm. Speckle images are acquired sequentially and the speckle intensity autocorrelation curves, $g_2(t)$, are calculated (box 1). The mean square displacements (MSD) of Brownian particles are deduced from the $g_2(t)$ curves, via a modified equation (box 2). Linear least square fitting to MSD yields the particles' diffusion coefficient, from which particle size is obtained as a function of imaging time (box 3).

A Camera Link cable transferred the speckle frames to a computer. For polystyrene microsphere suspensions, 500 frames were acquired, over an ROI of 500×500 pixels, every 30 seconds at 753 frames per seconds (fps), corresponding to 1.3 ms exposure time, for 20 minutes. For the PRP specimens, the speckle images were acquired over a smaller ROI of 200×200 pixels and more frequently in 15 seconds intervals, at significantly higher rate of 1808 fps, corresponding to 0.5 ms exposure time, to closely follow the more rapid kinetics of platelets. More specifically, we optimized the acquisition frame rate and exposure time to attain maximum temporal speckle contrast. Adequate temporal sampling of the speckle intensity fluctuations ensured that the speckle spots were not aliased and provided ample data points for deducing the mean square displacements (MSD) of scattering particles, as detailed below. To demonstrate the capability of laser speckle fluctuations for imaging and visualizing the platelet aggregate maps, the focusing lens in the optical setup was removed and PRP specimens from the second patient were evenly illuminated by a collimated beam (5 mm dia.). Magnified speckle images ($10 \times$) were acquired over an ROI of 5×5 mm, corresponding to 500×500 pixels, at 753 fps (with 1.3 ms exposure time), every 15 seconds for over 20 minutes.

2.4 Calculating the speckle intensity autocorrelation, $g_2(t)$

The time-resolved speckle intensity fluctuations are intimately related to the kinetics of the scattering particles and thus can be exploited to track the dynamics of activation and aggregation, as presented in the flowchart of Fig. 1(b). Briefly, cross-correlation analysis of speckle frames yielded the speckle intensity auto-correlation, $g_2(t)$, according to [15–17]:

$$g_2(t) = \left\langle \frac{\langle I(t_0)I(t_0 + t)\rangle_{pixels}}{\sqrt{\langle I(t_0)^2\rangle_{pixels}\langle I(t_0 + t)^2\rangle_{pixels}}} \right\rangle_{t_0} \tag{1}$$

where $I(t_0)$ and $I(t + t_0)$ represented speckle frames at times t_0 and $t + t_0$, $<>_{pixels}$ and $<>_{t0}$ stood for spatial and temporal averaging over the entire ROI and all the frames (imaging time of 0.66 s for polystyrene bead suspensions and 0.27-0.66 s for human PRP), respectively. Spatial and temporal averaging were performed to achieve sufficient statistical accuracy for calculating the $g_2(t)$ curves. During the time course of aggregation (20 minutes), a total of 41 and 81 $g_2(t)$ were processed for polystyrene bead suspensions and PRP specimens, respectively. To obtain the two-dimensional color-maps of MSD using the collimated beam illumination, spatial averaging in Eq. (1) was reduced to 25×25 Gaussian windows of neighboring pixels to cover an RoI of 500×500 corresponding to 5 mm $\times$ 5 mm area.

2.5 Extracting the MSD of scattering particles

To deduce the MSD of scattering particles from the $g_2(t)$, we noted that the specimens were neither optically dilute nor strongly scattering. Thus, we could not apply either of the single scattering or strong multiple scattering assumptions, i. e. dynamic light scattering (DLS) or diffusing wave spectroscopy (DWS) formalisms, to extract the MSD curves. Instead, a modified expression that we had previously derived using a correlation Monte-Carlo ray tracing algorithm was used as follows [11, 16, 17]:

$$g_2(t) = e^{-2\gamma\left(k_0^2 n^2 \langle \Delta r^2(t)\rangle\right)^{\varsigma}} \tag{2}$$

Here, $\langle \Delta r^2(t)\rangle$ represented the MSD, k_0 was the wave number, $n = 1.36$ was the refractive index of plasma, and γ and ζ were empirical parameters related to the optical properties of the specimen. Since knowledge of the reduced scattering coefficient, μ_s', was necessary to accurately evaluate the MSD of scattering particles, we used previously established methods that enable estimating the optical properties from the radial dependence of diffusely remitted intensity [11, 16–18]. To this end, the speckle image series were temporally averaged and converted to photon flux (i.e. photons per unit area) based on the camera responsivity, angle of view, and the area of illumination to yield the radial diffuse reflectance profile (DRP) during aggregation. Assuming that optical absorption was negligible, the DRP curves were fitted to a steady-state diffusion theory-based model to experimentally calculate the average μ_s' of each sample in the course of aggregation. In polystyrene bead suspensions, the average μ_s' values were calculated to be 1.6, 1.3, 1.1, and 0.8 mm^{-1} for MgCl$_2$ concentrations of 0, 5, 45, and 300 µM molar concentrations, resulting in (γ, ζ) pairs of (1.02, 0.8) for samples of 0, 5, and 45 µM, and (0.67, 1) for the specimen with 300 µM salt concentration. Since for PRP specimens, $\mu_s' = 0.02$ mm^{-1}, Eq. (2) converged to the DLS formalism with (γ, ζ) pair of (0.67, 1), i.e [14]:

$$g_2(t) = e^{\frac{-4}{3}k_0^2 n^2 \langle \Delta r^2(t)\rangle} \tag{3}$$

2.6 Extracting the aggregate size

Assuming that background water and plasma media in both polystyrene and PRP specimens were purely viscous, the MSD followed a linear trend, given by $\langle \Delta r^2(t)\rangle = 6Dt$, where D is the diffusion coefficient of particles. In these aggregating specimens, the diffusion coefficient of aggregating particles reduced and the particles executed increasingly sluggish Brownian displacements, decelerating the speckle fluctuations. The diffusion coefficient was obtained by linear least square fitting to the MSD curves and the standard Stokes-Einstein relation was used to return the size of Brownian particles, a, according to [19]:

$$a = \frac{K_B T}{6\pi\eta D} \tag{4}$$

where K_B was the Boltzman constant (1.38×10^{-23}), $T = 297°$ K ($24°$ C) was the absolute temperature (degrees Kelvin), a was the average sphere-equivalent radius of aggregates, and η was the viscosity of the medium. For polystyrene beads suspended in water, $\eta = 1$ mPa s. For PRP specimens, on the other hand, based on published data the viscosity of plasma was taken to be $\eta = 1.3$ mPa s [20]. Nevertheless, to prevent the influence of inter-patient variations in plasma viscosity, the calculated aggregate size was normalized to the baseline.

3. Results

3.1 Aggregation kinetics of polystyrene microsphere test phantoms

Figures 2(a)-2(d) displays the MSD curves, illustrating the Brownian displacements of polystyrene microspheres and aggregates, immediately following and after 20 minutes of salt activation for $MgCl_2$ concentrations of 0, 5, 45, and 300 µM, respectively.
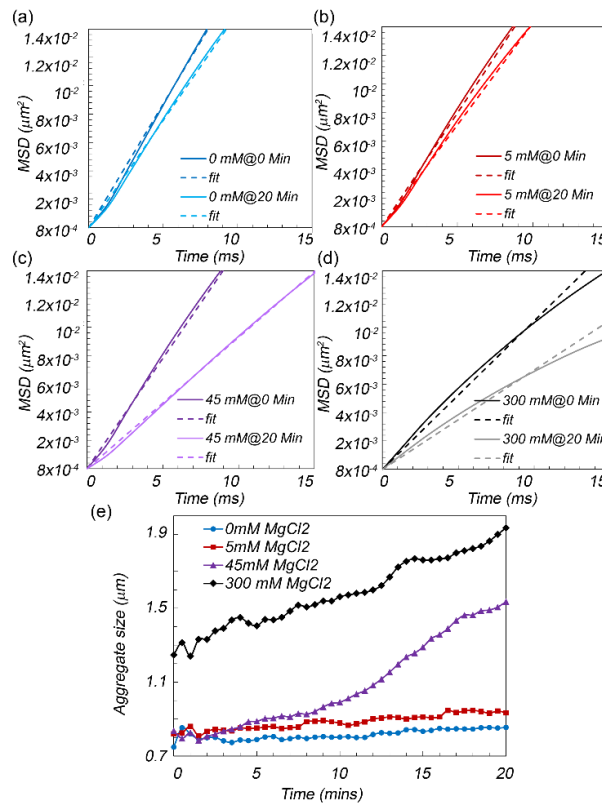

Fig. 2. (a-d) Mean square displacement (MSD) curves of aggregating polystyrene microspheres at 0 and 20 minutes after adding the $MgCl_2$ at 0, 5, 45, and 300 micromolar concentrations, respectively. The linear fits are also displayed with dashed lines. Clearly, the slope of MSD curves decreased following salt addition and this was more pronounced in higher salt concentrations, due to significantly faster aggregation and larger aggregate sizes. (e) Microsphere aggregate size as a function of time following the addition of salt. The aggregation rate and aggregate size increases with salt concentration.

These curves are obtained by substituting the values of (γ, ζ) pairs, corresponding to μ_s', deduced from the time averaged speckle patterns, in Eq. (2). The linear fits to MSD curves are also displayed with dashed lines. The MSD curves exhibit a nearly linear growth at early

times, illustrating diffusive particle motion in a simply viscous liquid [19]. Figure 2(e) depicts the trace line of polybead aggregate sizes in the first 20 minutes following the $MgCl_2$ addition. We observe that the average radii of aggregating polystyrene beads evolves from initial values of 0.75, 0.75, and 1.3 µm, at minute 0 to 0.9, 1.5 and 2.1 µm at minutes 20 for salt concentrations of 5, 45, and 300 µM, whereas zero to minimal aggregation is detected when no salt was present in the suspension. The larger radius of polybead aggregates at high salt concentrations is likely due to rapid initial aggregation, occurring immediately following sample preparation and prior to the start of speckle image acquisition.

3.2 Aggregation kinetics of PRP in response to agonists and anti-platelet drugs

Figures 3(a)-3(d) display the MSD of platelet aggregates at 15 seconds, 4 and 8 minutes following the addition of ADP and clopidogrel with molar concentration pairs of (0, 0 µM), (5, 0 µM), (5, 3 µM), and (5, 30 µM), depicted by the blue, red, purple, and grey curves, respectively. Moreover, the linear fits to the MSD curves are also displayed with dashed lines of similar colors.
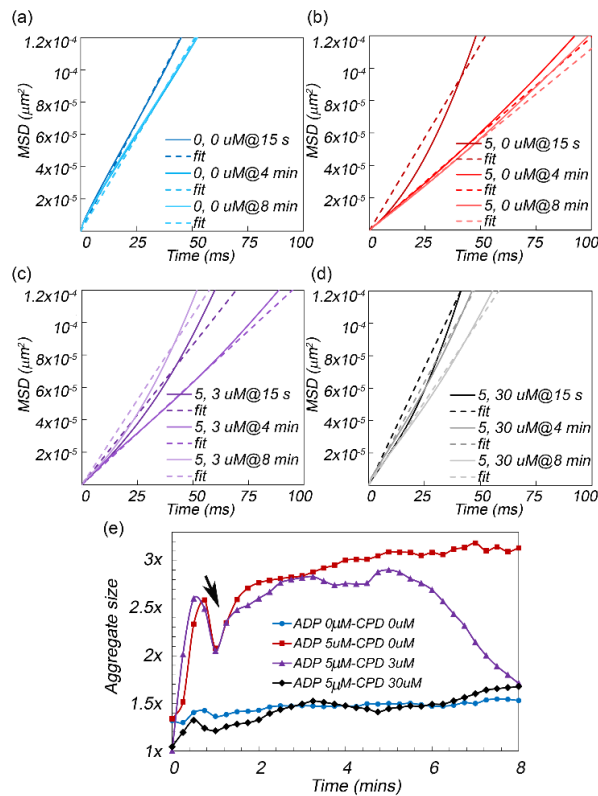

Fig. 3. (a) Mean square displacements (MSD) of platelets in platelet rich plasma (PRP) samples spiked with Adenosine Diphosphate (ADP) and Clopidogrel (CPD) concentrations of (a) ADP: 0µM, CPD 0 µM (blue curves), (b) ADP: 5µM, CPD 0 µM (red curves), (c) ADP: 5µM, CPD 3 µM (purple curves), and (d) ADP: 5µM, CPD 30 µM (grey curves), together with (e) trace-lines of platelet aggregate sizes in the four PRP samples. Zero to minimum platelet aggregation was observed in the absence of both ADP and CPD. By adding 5µM of ADP to plasma, a rapid and complete platelet aggregation was detected. With both 5µM ADP and 3µM CPD, the rapid initial aggregation was followed by a rapid disaggregation. Finally, by increasing the CPD concentration to 30 µM, no aggregation was observed.

It is observed that in the absence of ADP and clopidogrel, the MSD curves at different time points (Fig. 3(a)) are similar and grow with a steep slope, representative of the diffusive

motion of small individual platelets in nearly viscous plasma. When ADP is added at 5 µM concentration (Fig. 3(b)), the initial MSD behavior within 15 seconds following the start of speckle acquisition slightly slows down, perhaps due to platelet conformational changes that in effect increase the sphere-equivalent radii of individual platelets. This is followed by a significantly reduced slope of MSD at minutes 4 and 8, illustrating the sluggish Brownian displacements of aggregating platelets, formed in response to ADP addition. When clopidogrel is added at 3 µM concentrations (Fig. 3(c)), once again a small reduction is observed in the diffusive motion of platelets at early times, marking the brink of platelet activation, as above. Like the specimen spiked solely with ADP, a significantly lower MSD slope is also observed at minute 4, due to aggregate growth triggered by ADP. Nevertheless, at minute 8, the MSD curve exhibit a steep slope, resembling the dynamics of individual platelets, which suggest disaggregation and dissociation of platelets in response to the anti-platelet agent clopidogrel. Finally, when clopidogrel concentration is increased to 30 µM (grey curves), no significant change is observed in MSD trends at different time points, indicating near complete inhibition of platelet aggregation due to inhibition of the $P2Y_{12}$ platelet receptors and restricted aggregation by clopidogrel treatment.

Figure 3(e) depicts the corresponding trace lines of platelet aggregate size. These traces are calculated by first obtaining the diffusion coefficient of aggregates, D, from the linear least square fitting of MSD curves at each time point. Next, D and nominal plasma viscosity are replaced in Eq. (4) to yield the absolute aggregate size, a, for each time point. Finally, a values are normalized with respect to aggregate size at the initial time point, for all 4 samples. Clearly platelet aggregation kinetics change minimally in the control sample without the addition of ADP, indicating the absence of platelet aggregation, as evidenced by the nearly flat trace line (blue curve). By adding 5µM of ADP, a rapid increase in aggregation growth percent is observed within minutes (red curve). When 3 µM clopidogrel is added to ADP-activated PRP, the fast initial aggregation is reversed at minute 6, which points to the aggregation, followed by a quick disaggregation, in response to clopidogrel (purple curve). These results are corroborated by earlier reports on the mechanism of action of low-dose clopidogrel on platelet inhibition that demonstrate the disaggregation of platelets [21]. Finally, by increasing the clopidogrel concentration to 30 µM, only minor changes are observed in the aggregate size (black curve). For both ADP and clopidogrel concentration pairs of (5, 0) and (5, 3), we also observe a small dip in aggregation percentile around minute 1. This point likely marks the start of the secondary wave of aggregation (black arrow) as seen in LTA trace-lines for smaller ADP concentrations [5, 6, 10]. More specifically, at low ADP concentrations (typically 2.5-5 µM), the initial binding of ADP to $P2Y_1$ receptors leads to mobilization and release of intracellular calcium and a change in the shape of the platelets, which triggers the primary wave of aggregation. Nevertheless, effect of low dose ADP is reversible and a brief reduction in aggregate size may be observed in the trace-line. This brief decline may then be followed by the release of ADP from platelet storage granules and its binding to $P2Y_{12}$ receptors, which induce an upward inflection in the curve, manifesting the secondary and irreversible wave of full platelet aggregation. At higher ADP concentrations (typically 10 µM) such biphasic waveform is absent and the two waves of aggregation combine to form a single monotonically increasing trace-line, as discussed later. These results demonstrate that the laser speckle-based approach accurately quantifies the modulation of aggregate growth in response to ADP and clopidogrel titrations and thus establish the suitability of this technique for platelet aggregometry.

3.3 Mapping the local aggregation dynamics

As detailed above, the expanded beam illumination in conjunction with spatio-temporal analysis of speckle intensity fluctuations allowed us to evaluate the $g_2(t)$ for each pixel of the speckle frame series, acquired from PRP specimens. The $g_2(t)$ curves were processed according to the flowchart of Fig. 1(b) to obtain the MSD of aggregates, the scattering signal of

which was mapped to the pixels of frame series. Figure 4 displays the MSD values, at the lag time of 100 ms, in the control PRP specimen as well as the one activated with 10 μM ADP, at 0 seconds, 15 seconds, and 8 minutes following activation.
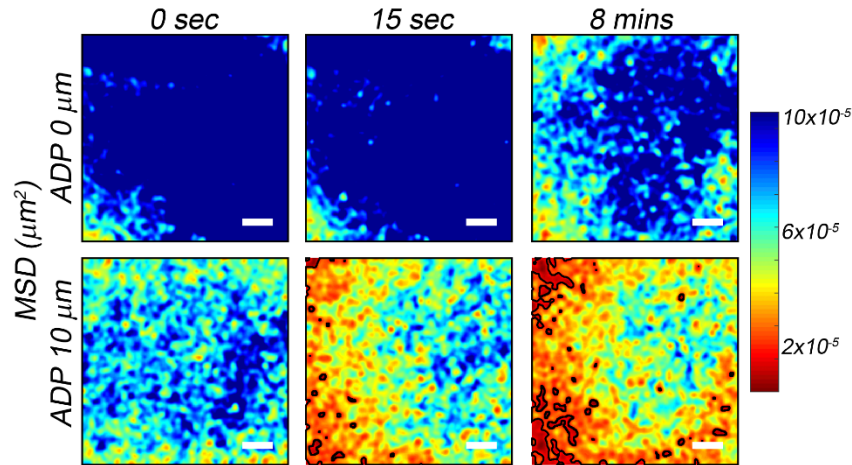

Fig. 4. Spatial maps of MSD at the lag time of 100 ms in PRP samples in the absence of ADP agonist (top row) and when spiked with 10 μM of ADP (bottom row) at 0 seconds, 15 seconds, and 8 minutes following activation. Aggregation foci of significantly reduced MSD appear within seconds of adding the ADP agonist, as evidenced in the bottom panels. These results demonstrate the high sensitivity and spatial resolution for detecting incipient hemostatic plugs from laser speckle fluctuations during very early stages of platelet aggregation. Scale bars are 500 μm.

Clearly, the MSD values reduce rapidly and significantly following the addition of high concentration ADP in the test PRP specimens and aggregation foci are spotted as early as 15 seconds, followed by propagation of the hemostatic plug in the subsequent minutes. In contrast, only minimal aggregation and MSD reduction is detected at much later times in the control PRP specimens, likely caused by residual activation of platelets due to shearing induced by pipetting the specimen into the imaging chamber. These results, demonstrate the ability to detect and visualize early platelet aggregates in small PRP sample volumes from laser speckle fluctuations, otherwise imperceptible by currently available platelet function testing devices. Moreover, the results together highlight the acute sensitivity of this approach to early aggregation and the capability to provide a portrait of platelet health and function in a matter of a few seconds. The invaluable diagnostic potential of laser speckle dynamics may help with immediate decision-making about the type and dose of antiplatelet therapy in the interventional cardiology suite at or near the patient bedside.

4. Discussion

We demonstrated the potential of exploiting laser speckle intensity fluctuations for testing the platelet function, by measuring various phases of primary platelet plug formation. Laser speckle fluctuations exhibited exquisite sensitivity to diffusive Brownian dynamics of scattering centers in both polystyrene microsphere suspensions and PRP specimens, which enabled tracking the activation and aggregation kinetics as evidenced by Figs. 2 and 3. Moreover, the potential of laser speckle dynamics for imaging and visualization of aggregation foci enabled inspecting early aggregate formation during initial stages of the primary coagulation process at a significantly shorter time compared to currently available platelet function testing devices.

In the current study, the optical setup illuminated the samples with both focused and collimated beams. At 632nm, $\mu_a = 0.00165$ mm^{-1} for plasma and $\mu_a \sim 0$ for polystyrene beads. Thus, the irradiance caused by focusing the beam to a 50 μm diameter spot, did not warm up

the samples to the extent that could alter their physiological and physical properties or affect the accuracy and reproducibility of results. For plasma, the small dimensions of the imaging chambers compared to the absorption length, $l^a = 1/\mu_a = 606$ mm, made it highly unlikely that a significant amount of light was absorbed. Besides, since the mean free path, $l^* = 1/\mu_s' = 50$ mm, was also very large, the odds of photon absorption in longer optical paths resulting from multiple scattering was also negligible. We experimentally verified temperature stability during imaging, by simultaneously logging the temperature within a test and a control imaging chamber loaded with human plasma, every 10 seconds, for 15 minutes, via a dual-channel digital thermometer (TMD-56, Amprobe), and two bead type thermocouples. The test sample was placed in the beam path (632 nm, 2 mW, 50 μm spot diameters) and the control was kept away from the illumination beam. A two-way ANNOVA analysis confirmed that there was no difference between temperatures of test and control chambers (p = 0.89) and that the temperature of the chambers did not change significantly over time (p = 0.506). These observations were further corroborated by comparing the data obtained using the focused and collimated beams, which indicated that both illuminations provided similar trace-lines of platelet aggregate size growth, asserting that the focused beam did not influence the optical and physiological properties of plasma. Similar temperature stability during imaging was expected in the polystyrene samples, given $\mu_a = 0$.

In the current optical setup, the iris in the imaging lens was adjusted to image a single speckle to 5x5 = 25 pixels, as confirmed by calculating the spatial autocorrelation function of speckle images and measuring the spatial correlation distance. This exceeded the requirements of Nyquist sampling theorem, i.e. pixel to speckle ratio of 2x2 = 4, and guaranteed that speckle spots were not aliased. Similarly, in the temporal domain, the high frame rates of 753 and 1808, for imaging polystyrene beads and platelets, prevented the integration of multiple speckle realizations into a single frame and the subsequent aliasing and smearing of the speckle spots. The sufficiency of acquisition frame rate was confirmed by calculating the temporal contrast of speckle intensity fluctuations, according to $K = \sigma_I^2/\mu_I^2$ and ensuring that K~1.

The linear polarizer in the optical setup eliminated majority of high intensity specular reflection. Nevertheless, surface roughness of polycarbonate windows, covering the chamber, could occasionally create a residual non-fluctuating speckle. This non-fluctuating component only slightly increased the $g_2(t)$ plateau level. The plateau artifact did not influence the initial speckle decorrelation or the MSD, used to deduce the aggregate size and thus did not affect the results. However, one could completely eliminate the background non-fluctuating speckle by reviewing the temporal statistics of individual pixels within the frame series and removing the pixels that exhibit the lowest temporal variations, with minimal intensity standard deviation, i.e. σ_I^2. An oblique collection could also reduce the specular reflection. However, for the single-scattering limit, $g_2(t) = exp(-2/3k^2(1-cos\theta)<\Delta r^2(t)>)$, where k is the wave number and θ is the collection angle, deviation from 180° back-scattering would complicate the extraction of MSD from the $g_2(t)$ curve. This is because, for $\theta \neq 180°$, it is challenging to tightly control the angle and avoid alterations in the $g_2(t)$ expression and discrepancies in the measured MSD. Moreover, the $g_2(t)$ decay rate reduces when $\theta \neq 180°$, requiring longer speckle acquisition to capture the full extent of particle displacements. This is impractical in the context of platelet aggregation monitoring, where rapid intermittent time-lapse speckle acquisitions are required to track the rapidly evolving Brownian motion dynamics.

When analyzing the speckle dynamics, we assumed that particles experience purely diffusive Brownian excursions in a simple viscous fluid. This was perfectly valid for individual platelets and polystyrene microsphere, where a~1μm. As platelets and beads aggregate, and the aggregates grow, gravitational sedimentation could introduce a deterministic downward displacement. In characterizing this motion, we note that the settling velocity, or sedimentation rate is given by, $v_s = 2(\rho_{particle}-\rho_{media})ga^2/9\eta$, where ρ is density, g is the gravitational acceleration, a is the particle radii, and η is the viscosity of the media. For both platelets floating

in plasma and polystyrene microspheres in water, the v_s = 1.3 µm/min. Thus, the excess MSD increment due to sedimentation at the lag time of t = 100ms, is $v_s^2 t^2$ = 4.7x10^{-6} µm^2, which is far below the MSD due to Brownian diffusion. In principle, for very large aggregates with radii of several tens of micrometers, the influence of sedimentation could become more pronounced. Nevertheless, for the aggregate sizes measured in our study, the trends and values reported for MSD in Figs. 2(a)-2(d), 3(a)-3(d), and 4 did not exhibit evidence of additional movements due to sedimentation. In particular, for aggregating platelets the MSD values at the lag time of 100 ms (Figs. 3 and 4), were reduced one order of magnitude, consistent with slowly decaying Brownian diffusion rate in response to aggregation. On the contrary, if the motion due to sedimentation was to be influential in the MSD trends, we should have observed a rapid and steady increase in the MSD values, raising from as low as 4.7x10^{-6} µm^2 for individual platelets to 4.7x10^{-2} µm^2 for aggregates of 10 micron radius. Other dynamic light scattering studies suggest that non-random motions due to sedimentation could only affect the $g_2(t)$ at significantly longer lag times, by inducing episodes of abrupt spikes in the plateau [22]. Therefore, in the current manuscript, a linear model was fitted to MSD of polystyrene beads and platelets over the first 10 and 100 milliseconds, respectively, to nearly isolate the Brownian excursions from deterministic sedimentation motion. As it is evident from Figs. 2(e) and 3(e), we could successfully track polystyrene aggregates of up to 2.5 µm and platelet aggregates of up to 3x larger than individual platelets. Moreover, the aggregate maps of Fig. 4, revealed that we could spot aggregate foci, with significantly reduced MSD values (corresponding to a few 10s of microns in particle radii), consistent with previous scanning electron microscopy (SEM) measurements [23].

In this study, we first quantitatively compared the laser speckle approach with a reference standard by evaluating the aggregation of mono-disperse polystyrene microsphere suspensions of known radii. The microsphere size, estimated from laser speckle fluctuations, closely agreed with manufacturer's specifications (Fig. 2). However, similar comparisons of platelet aggregate size with a standard-reference were not possible in this study. This is because the current standard-reference technique, LTA for platelet aggregometry reports the relative change in the transmitted light intensity, following the addition of agonist, as a surrogate metric of platelet aggregation and does not provide a direct quantification of aggregate size. In contrast, the laser speckle approach directly quantifies the actual change in aggregate radii. Therefore, a direct one-to-one comparison of platelet aggregate growth was not possible. Instead, we have shown that expected trends of platelet aggregation and inhibition are quantified using the speckle approach, exhibiting similar trends as measured in the literature using LTA [5, 6, 21]. For instance, in Fig. 3(e), platelet aggregation began promptly following the addition of ADP, indicating immediate activation, consistent with what is typically seen in LTA trace-lines for this agonist [10]. At critical concentrations of ADP (between 2 and 5µM, as in the current study), LTA measurements often report a biphasic platelet aggregation trend [10]. Immediately following addition of ADP, the agonist binds to the P2Y$_1$ receptor, causing platelet to go through conformational change in shape and size with a corresponding appearance of pseudopodia, which together may increase the scattering cross-section [3]. The corresponding increase in plasma turbidity is demarcated by a notch in typical LTA curves and is highlighted by a decelerated MSD in laser speckle based measurements. This is rapidly followed by an initial wave of aggregation seen at time 15s in Fig, 3(e), (termed the primary wave), consistent with the well-known LTA reports. This phase is reversible at low ADP concentrations and a rapid and brief disaggregation of platelets may be seen at the end of the primary wave, consistent with the dip at time 1:30 minutes in Fig. 3(e). The timing of the recovery from this dip, coincides with the brief upward deflection, commonly seen in the LTA traces, at the end of the primary wave, when ADP is released from platelet storage granules and binds to the primary ADP receptor, P2Y$_{12}$, causing rapid increase in platelet aggregation (referred to as the secondary phase) as observed between time 1:30 and 2:00 minutes and marked by the black arrow in Fig. 3(e), accentuating a primary and a secondary slowdown of speckle

dynamics. The $P2Y_{12}$ receptor is the target of multiple anti-platelet drugs, including clopidogrel (Plavix), which inhibits the aggregation irreversibly [10, 21, 24]. LTA studies on the response to clopidogrel demonstrated that when platelets were incubated with clopidogrel, maximum ADP-induced aggregation was gradually reduced in concert with clopidogrel concentration [21, 24, 25]. Moreover, the initial aggregation was reversed within minutes following the addition of ADP [21]. The purple and black trace-lines of Fig. 3(e) closely mirror the results of these past studies, for moderate (3 µM) and high (30 µM) concentrations of clopidogrel [21, 24]. More specifically, while the maximum aggregation percentile remains nearly unchanged when only 3 µM of clopidogrel is added to the ADP-stimulated PRP sample, the aggregation is entirely diminished when clopidogrel concentration is raised to 30 µM. The above results demonstrated the capacity for accurate quantification of aggregate size modulation in response to dose-dependent treatment with platelet agonists and antagonist such as ADP and clopidogrel.

The laser speckle aggregometry approach likely offers several major improvements over LTA, by directly evaluating the aggregate growth, via illuminating two drops of plasma with a laser beam and imaging the back-scattered laser speckle intensity fluctuations. Platelet function testing is often required in severely bleeding patients with low CBC counts. As a results, blood-conserving techniques that require small sample volumes are imperative in such patients. The capability to assess platelet function in a small sample volume is thus a major advantage of our approach, compared to LTA.

Alternative platelet function assays that circumvent the limitations of LTA have been recently investigated. For instance, a promising new technique has been proposed for exploring a flow-cytometry based assay to evaluate the P-selectin (a cell-adhesion molecule) expression as an indicator of platelet function [26]. This method however requires extensive sample preparation, an expensive instrument (flow cytometer), and experienced technicians for interpreting the results, which may somewhat limit its widespread clinical adoption. Other FDA approved devices, such as VerifyNow, multiplate aggregometry and Thromboelastography (TEG), provide key quantifiable metrics for assessing platelet health and response to anti-coagulant therapies [27–30]. Nevertheless, majority of these techniques remain less prevalent than LTA, as they currently only portray a static snap-shot of overall platelet function, and report a digital pass or fail diagnostic, but fall short of providing critical identifiers of specific platelet defects, such as platelet shape change, the occurrence of secondary wave of aggregation or platelet de-aggregation [7]. The laser speckle approach, on the other hand, offers a simple and elegant optical setup along with a novel speckle processing scheme for inexpensive platelet function testing from two drops of plasma in a fraction of time required by other alternatives. Moreover, the speckle data may be easily interpreted both as a trace line, like LTA, and a color-map for visualizing incipient platelet aggregates with high resolution. The imaging capabilities opens new avenues for rapid monitoring of platelet health and function, beyond what is currently available by alternative techniques

5. Conclusion

In conclusion, the demonstrated acute sensitivity of the laser speckle approach to early phases of aggregation and the capability to profile platelet health underscore the diagnostic potential of this technique. The laser speckle approach presented here holds the promise to be integrated via simplified and compact instrumentation for use at the point-of-care in various clinical settings for managing cardiovascular disease, trauma patients, and monitoring anti-coagulation therapies.

Funding

Acknowledgments

Disclosures